Steady-state properties of a nonequilibrium Fermi gas

Pedro Ribeiro*

CeFEMA, Instituto Superior Técnico, Universidade de Lisboa, Avenida Rovisco Pais, 1049-001 Lisboa, Portugal

(Received 10 June 2016; revised manuscript received 3 July 2017; published 2 August 2017)

The current-carrying steady state that arises in the middle of a metallic wire connected to macroscopic leads is characterized regarding its response functions, correlations, and entanglement entropy. The spectral function and the dynamical structure factor show clear nonequilibrium signatures accessible by state-of-the-art techniques. In contrast with the equilibrium case, the entanglement entropy is extensive with logarithmic corrections at zero temperature that depend on the lead-wire coupling and, in a nonanalytic way, on voltage. This shows that some robust universal quantities found in gapless equilibrium phases do not persist away from equilibrium.

DOI: 10.1103/PhysRevB.96.054302

I. INTRODUCTION

Current-carrying steady states (CCSS) are characterized by a steady flow of equilibrium-conserved quantities, such as energy, spin, or charge. Of direct relevance to transport experiments are steady currents generated by coupling a system to reservoirs at different thermodynamic potentials. The resulting CCSS are thermodynamically unbalanced, i.e., do not fulfill equilibrium fluctuation-dissipation relations [1,2]. CCSS in one- or quasi-one-dimensional systems are of relevance in many fields, including charge and spin transport in electronic devices and in cold-atom setups.

Due to kinetic constraints, accounting for relaxation in one dimension requires one to go beyond two-body interaction terms and explicitly account for three- and higher-body collisions [3–5] and thus may be neglected for weakly interacting clean samples. For noninteracting electrons on a wire, ideal reservoirs can be mimicked by injecting particles from plus and minus infinity with given energy distributions [6–9]. These ideal conditions, alluded to as Landauer reservoirs [10,11], yield to a local energy distribution function that is the average of those of the leads. A series of studies featuring nonequilibrium Luttinger liquids [12–17] found that interaction-induced dephasing may smear the local energy distribution even in the absence of relaxation. In the presence of a strong enough relaxation, the system is expected to equilibrate locally. Treatments based on the Boltzmann equation have been used to obtain the distribution function of the charge carriers in this regime [3–5,18–20].

Experiments featuring CCSS, designed to access the local energy distribution of charge carriers, were performed using tunneling spectroscopy in mesoscopic wires [21–23] and carbon nanotubes [24]. The local energy distribution, measured in the center of the wire, was reported to exhibit a characteristic double-step form resulting from contribution of both Fermi functions of the electronic leads. The sharp steps seen at low temperatures are smeared out as temperature increases or in the presence of electron-electron interactions, disorder, or electron-phonon coupling.

The study of current-carrying states recently became available for cold-atomic setups [25]. Mainly motivated by these advances, a rather different body of works investigated the time evolution of two initially disconnected semi-infinite wires held at different equilibrium conditions. After the two wires are connected, a CCSS forms around the connection point. This central region grows with time, with the remaining parts of the wire acting essentially as reservoirs. At large times, a translationally invariant CCSS is locally observed [26–35], as long as the chains are not in a correlated insulating state [36]. Interestingly, some of the properties of the CCSS created in this way, in particular the momentum-resolved electronic distribution, are similar to the CCSS obtained using a Landauer description [26,29–33,37–39]. Furthermore, in both cases, the entanglement entropy of a region in the middle of the wire yields to the same universal result as in equilibrium.

Recently, momentum-resolved spectroscopic measurements became available for nonequilibrium electronic systems [40,41]. Since the same local energy spectrum may correspond to various momentum distributions, these developments allows a better characterization of the state and may shed some light on discrepancies between existing theoretical predictions and experimental findings. In addition, transport experiments in cold-atomic setups [25] allow one to access a set of physical quantities that are difficult to study in solid-state devices. These developments urge for a better theoretical understanding of thermodynamically unbalanced CCSS, beyond the local energy distribution function, that is currently still unavailable.

This work addresses the CCSS realized on a finite metallic wire coupled to metallic leads at different temperatures and chemical potentials. The lead-wire couplings are treated explicitly as they induce additional reflections that change the energy distribution of the carriers [6,7]. At equilibrium, the system can be described by a one-dimensional electron gas as we assume no electron-electron interactions or disorder to be present. These assumptions hold for weakly interacting clean systems when the system size is larger than the disordered-induced localization length, and the equilibrium Luttinger parameter [42] used to model the interactions is close to unity. Our approach describes the low-energy sector where the dispersion relation is essentially linear and the reservoirs' chemical potentials and temperatures are much smaller that the wire's bandwidth. We study the one- and two-point functions and analyze the entanglement content in the wire's central region.

*ribeiro.pedro@gmail.com

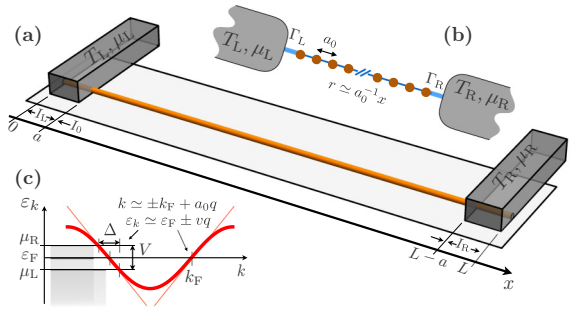

FIG. 1. (a) Schematics of the setup. (b) Tight-binding chain coupled to reservoirs. (c) Dispersion relation of the tight-binding chain, ε_k, linearized around the Fermi momentum, k_F, defined such that $\varepsilon_{k_F} = (\mu_L + \mu_R)/2$, with $V = \mu_L - \mu_R$ and $\Delta = a_0 V/v$.

II. MODELS

Consider the setup of Fig. 1(a) depicting a one-dimensional fermionic gas on a wire of length L attached to external leads. In the wire, we assume fermions to have an approximately linear dispersion, with velocity v, within a window of size 2Λ around the Fermi points. The effective Hamiltonian of the isolated metallic wire, valid for energies scales below $v\Lambda$, is given by

$$H = -iv \int dx\, \Psi^\dagger(x) \sigma_z \partial_x \Psi(x), \tag{1}$$

where $\Psi(x) = \{\psi_L(x), \psi_R(x)\}^T$, with $\psi_{l=L,R}(x)$ corresponding to the left- and right-moving fermions with $\{\psi_l(x), \psi_{l'}^\dagger(x')\} = \delta_{ll'}\delta(x-x')$. At position $x_L = 0$ and $x_R = L$, the boundary conditions are given by $\psi_L(x_l) = e^{i\phi_l}\psi_R(x_l)$ with phase shift ϕ_l. To model the leads, we assume that the extremities of the wire are connected to fermionic reservoirs within a region of length $a \ll L$, such as in Fig. 1(a). The reservoirs are assumed to be metallic, with a bandwidth much larger than any characteristic energy scale of the wire. Their chemical potentials $\mu_{l=L,R}$ and temperatures $T_{l=L,R} = \beta_{l=L,R}^{-1}$ are taken to be much smaller than the energy cutoff $v\Lambda$. The system-reservoir coupling, given by $H_{S\text{-}R} = \sum_{l=R,L} t_l \int_{I_l} dx\, [\Psi^\dagger(x)\Psi_l(x) + \text{c.c.}]$, where $\Psi_l(x)$ is a fermionic field of lead l, induces a hybridization between the wire and the lead characterized by the energy $v\gamma_l = \pi(at_l)^2 \nu_l$, which is proportional to the square of the hopping amplitude per unit length t_l from region I_l to lead l and to the lead's density of states ν_l. The corresponding time scale $(v\gamma_l)^{-1}$ gives the characteristic time for a particle in region $I_{l=L,R}$ to escape the reservoir l. With these assumptions, integrating out reservoir l yields a self-energy contribution to the propagator of the system, with retarded (R) and advanced (A) components given by

$$\Sigma_l^{R/A}(\omega; xx') = \mp i\delta(x-x')v\,\gamma_l \Theta[|x-x_l| - a], \tag{2}$$

where $\Theta(x)$ is the Heaviside theta function. Since the reservoirs are taken to be at thermal equilibrium, the Keldysh (K) component is

$$\Sigma_l^K(\omega; xx') = \tanh\left[\frac{\beta_l}{2}(\omega - \mu_l)\right]\left[\Sigma_l^R(\omega; xx') - \Sigma_l^A(\omega; xx')\right]. \tag{3}$$

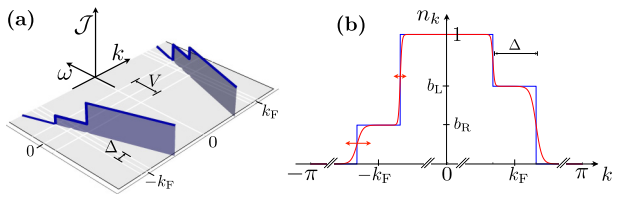

FIG. 2. (a) $\mathcal{J}_k(\omega) = -i\frac{1}{2\pi}G_k^<(\omega)$, proportional to the transition rate measured by angle-resolved photoemission spectroscopy, for $T_L, T_R = 0$. (b) Momentum-resolved occupation number n_k given for $T_L = T_R = 0$ (blue) and $T_L > T_R \neq 0$ (red).

The total self-energy is the sum of the contributions of both reservoirs $\mathbf{\Sigma}^{R/A/K} = \sum_l \mathbf{\Sigma}_l^{R/A/K}$. In the following, we set $\mu_L - \mu_R = V \geqslant 0$ without loss of generality.

In addition to the low-energy model above, we present a set of numerical results for a tight-binding model on a chain of N sites, with Hamiltonian

$$H_{TB} = -t\sum_{r=1}^{N} c_r^\dagger c_{r+1} + \text{H.c.}, \tag{4}$$

coupled at the two end sites to a wideband reservoir, as in Fig. 2(b). The reservoir l introduces a hybridization energy scale $\Gamma_l = \pi t_l^2 D_l$, where t_l is the chain-reservoir hopping and D_l is the local density of states of the reservoir. This yields to a self-energy contribution from the reservoir l given by

$$\Sigma_{TB,rr';l}^{R/A}(\omega) = \mp i\Gamma_l \delta_{r'r_l}\delta_{rr_l}, \tag{5}$$

with $r_L = 1$ and $r_R = N$. The Keldysh component is obtained from $\Sigma^{R/A}$ as in the continuum case.

The correspondence between the low-energy sectors of these two models (see Appendix A) allows for a detailed comparison of analytical results, obtained for the continuum model, and numerics done for the tight binding that provide the following identifications. The average Fermi momentum k_F is defined such that $\varepsilon_{k_F} = \varepsilon_F = (\mu_L + \mu_R)/2$, thus for q smaller than Λ: $\varepsilon_k \simeq \varepsilon_F \pm vq$ and $c_r \simeq e^{ik_F r}\psi_L(a_0 r) + e^{-ik_F r}\psi_R(a_0 r)$, with $k = \pm k_F + a_0 q$ and a_0 the lattice constant; see Fig. 2(c). Further identification between the continuum and tight-binding models yield to $N = La_0^{-1}$, $k_F = \arccos(-\varepsilon_F/2t)$, $v = 2a_0 t \sin k_F$.

III. METHOD

In order to address the properties of the steady state that forms under the conditions described above, we compute the retarded (R), advanced (A), and Keldysh (K) components of the Green's function in the frequency domain. The wideband nature of the reservoirs considerably simplifies our treatment [43]. In this case, the retarded Green's function is given by

$$\boldsymbol{G}^R(\omega; x, x') = \langle x|(\omega - \boldsymbol{K})^{-1}|x'\rangle, \tag{6}$$

where

$$\boldsymbol{K} = -iv\int dx\, |x\rangle\left[\sigma_z\partial_x + \sum_{l=L,R}\gamma_l\Theta[|x-x_l|-a]\right]\langle x| \tag{7}$$

is a non-Hermitian operator describing a single particle on a wire with particle sinks in regions $I_{l=\mathrm{R,L}}$, with boundary conditions imposed by the reservoir-free system: $\boldsymbol{S}_l\langle x_l|\psi\rangle = \langle x_l|\psi\rangle$, where

$$\boldsymbol{S}_l = \begin{pmatrix} 0 & e^{i\phi_l} \\ e^{-i\phi_l} & 0 \end{pmatrix}. \tag{8}$$

$\boldsymbol{K}$ is diagonalized by left and right eigenvectors $\langle\tilde{\psi}_n|$ and $|\psi_n\rangle$, with eigenvalues $\lambda_n = vq_n$. In position space, $\langle\tilde{\psi}_n x\rangle$ and $\langle x|\psi_n\rangle$ are plane waves, with a complex-valued momentum q_n, for x within the regions $I_{l=\mathrm{R},0,\mathrm{L}}$ defined in Fig. 1(a). The wave amplitudes within each region are given by

$$\langle x \in I_{\mathrm{L}}|\psi\rangle = \frac{1}{\sqrt{2L}}\begin{pmatrix} e^{(a-x)\gamma_{\mathrm{L}}+iqx} \\ e^{(a+x)\gamma_{\mathrm{L}}-i(\phi_{\mathrm{L}}+qx)} \end{pmatrix}, \tag{9}$$

$$\langle x \in I_0|\psi\rangle = \frac{1}{\sqrt{2L}}\begin{pmatrix} e^{iqx} \\ e^{-i(2ia\gamma_{\mathrm{L}}+\phi_{\mathrm{L}}+qx)} \end{pmatrix}, \tag{10}$$

$$\langle x \in I_{\mathrm{R}}|\psi\rangle = \frac{1}{\sqrt{2L}}\begin{pmatrix} e^{-\gamma_{\mathrm{R}}(a-L+x)+iqx} \\ e^{-\gamma_{\mathrm{R}}(a+L-x)+i(2Lq-qx-\phi_{\mathrm{R}})} \end{pmatrix}, \tag{11}$$

and

$$\langle\tilde{\psi}|x \in I_{\mathrm{L}}\rangle = \frac{1}{\sqrt{2L}}\begin{pmatrix} e^{(x-a)\gamma_{\mathrm{L}}-iqx} \\ e^{i[i(a+x)\gamma_{\mathrm{L}}+\phi_L+qx]} \end{pmatrix}^T, \tag{12}$$

$$\langle\tilde{\psi}|x \in I_0\rangle = \frac{1}{\sqrt{2L}}\begin{pmatrix} e^{-iqx} \\ e^{i(2ia\gamma_{\mathrm{L}}+\phi_{\mathrm{L}}+qx)} \end{pmatrix}^T, \tag{13}$$

$$\langle\tilde{\psi}|x \in I_{\mathrm{R}}\rangle = \frac{1}{\sqrt{2L}}\begin{pmatrix} e^{\gamma_{\mathrm{R}}(a-L+x)-iqx} \\ e^{\gamma_{\mathrm{R}}(a+L-x)-2iLq+iqx+i\phi_{\mathrm{R}}} \end{pmatrix}^T, \tag{14}$$

and the quantization condition $q_n \equiv -\frac{1}{2L}(\phi_{\mathrm{L}} - \phi_{\mathrm{R}}) + \frac{\pi n}{L} - ia\frac{\gamma_{\mathrm{L}}+\gamma_{\mathrm{R}}}{L}$, with $n \in \mathbb{Z}$, are determined by imposing boundary conditions at $x = 0, L$, the continuity of the wave functions at $x = a, L-a$, and the normalization of the wave functions $\langle\tilde{\psi}_n|\psi_{n'}\rangle = \delta_{nn'}$. The retarded Green's function, in terms of these single-particle quantities, gives $\boldsymbol{G}^R = \sum_n |\psi_n\rangle(\omega - vq_n)^{-1}\langle\tilde{\psi}_n|$. The Keldysh component of the Green's function in the steady state, given by $\boldsymbol{G}^K = \boldsymbol{G}^R\boldsymbol{\Sigma}^K\boldsymbol{G}^A$, can also be obtained explicitly using essentially the same procedure. For convenience, in the following we analyze the Hermitian matrices $\boldsymbol{\rho}^- = -[\boldsymbol{G}^R - \boldsymbol{G}^A]/2\pi i$ and $\boldsymbol{\rho}^+ = \boldsymbol{G}^K/(-2\pi i)$ rather than the Green's functions. The explicit expressions of $\langle x|\boldsymbol{\rho}^{\pm}|x'\rangle$ are given in Appendix B.

In order to compare results from the continuum and tight-binding models, the phase shifts in Eq. (8) and the relation between the hybridization Γ_l and the parameter γ_l have to be determined; this is done in Appendix C. The phase shifts, $\phi_{\mathrm{L}} = 2k_{\mathrm{F}} - \pi; \phi_{\mathrm{R}} = -2k_{\mathrm{F}}La_0^{-1} - \pi$, are obtained by analyzing the tight-binding eigenfunctions near the boundaries in the absence of the leads. The relation

$$a\gamma_l = \frac{1}{4}\ln\left(-\frac{\Gamma_l^2 t^{-2} - 2t^{-1}\sin k_{\mathrm{F}}\Gamma_l + 1}{\Gamma_l^2 t^{-2} + 2t^{-1}\sin k_{\mathrm{F}}\Gamma_l + 1}\right) \tag{15}$$

between hybridization constants can be derived by matching the imaginary part of the wave vectors. A numerical comparison between the two models is given in Appendix C 3.

IV. RESULTS

A. Single-particle correlation functions

We concentrate in the middle region of the wire in the limit $L \to \infty$, in which case the quantities $\boldsymbol{\rho}^{\pm}_{\mathrm{bulk}}(\omega; x, x') \equiv \lim_{L\to\infty}\boldsymbol{\rho}^{\pm}(\omega; x + L/2, x' + L/2)$ become translationally invariant, for finite x and x', and their Fourier components are given by

$$\boldsymbol{\rho}^{\pm}_{\mathrm{bulk}}(\omega,q) = \mathrm{diag}\{\rho^{\pm}_{\mathrm{L}}(\omega,q), \rho^{\pm}_{\mathrm{R}}(\omega,q)\}, \tag{16}$$

with $\rho^{-}_{\mathrm{L/R}}(\omega,q) = \delta(\omega \mp vq)$ and $\rho^{+}_{l}(\omega,q) = [1 - 2n_l(\omega)]\rho^{-}_{l}(\omega,q)$, for $|q| < \Lambda$, and where

$$n_l(\omega) = \frac{b_l}{e^{\beta_l(\omega-\mu_l)}+1} + \frac{(1-b_l)}{e^{\beta_{\bar{l}}(\omega-\mu_{\bar{l}})}+1} \tag{17}$$

is the energy distribution function of the l movers, with $\bar{R} = L$, $\bar{L} = R$, $a\gamma_{\mathrm{L}} = \frac{1}{4}\ln\frac{1-b_{\mathrm{R}}}{1-b_{\mathrm{L}}}$ and $a\gamma_{\mathrm{R}} = \frac{1}{4}\ln\frac{b_{\mathrm{L}}}{b_{\mathrm{R}}}$. Since $V \geqslant 0$, we have that $b_{\mathrm{L}} \geqslant b_{\mathrm{R}}$. Using the correspondence with the continuum model, the tight-binding Green's functions $G^{\alpha}_{rr'}(\omega)$ or, equivalently, the quantities $\rho^{\pm}_{rr'}(\omega)$ are given by $\rho^{\pm}_{rr'}(\omega) = \int_{-\pi}^{\pi}\frac{dk}{2\pi}\rho^{\pm}_k(\omega)e^{ik(r-r')}$, for r and r' in the middle of the wire, where

$$\rho^{\pm}_k(\omega) = \rho^{\pm}_{\mathrm{L}}\left[\omega,(k-k_{\mathrm{F}})a_0^{-1}\right]\Theta(|k-k_{\mathrm{F}}| - \Lambda a_0) + \rho^{\pm}_{\mathrm{R}}(\omega,k+k_{\mathrm{F}})\Theta(|k+k_{\mathrm{F}}| - \Lambda a_0). \tag{18}$$

Due to the quadratic nature of the model, these quantities can be used to compute all correlations and response functions restricted to the center of the wire and to low energies. In particular, the single-particle density matrix $\varrho_{rr'}(t) = \langle c^{\dagger}_r(t)c_{r'}(t)\rangle$, which in the steady state is given by $\varrho_{rr'} = -\pi\int\frac{d\omega}{2\pi}\rho^{+}_{r'r}(\omega) + \frac{1}{2}\delta_{rr'}$, can be approximated by

$$\varrho_{rr'} \simeq \varrho_{r-r'} = \int_{-\pi}^{\pi}\frac{dk}{2\pi}e^{-i(r-r')k}n_k, \tag{19}$$

with

$$n_k = n_{\mathrm{L}}\left[\frac{v}{a_0}(k-k_{\mathrm{F}})\right]\Theta(|k-k_{\mathrm{F}}| - \Lambda a_0) + n_{\mathrm{R}}\left[\frac{v}{a_0}(-k_{\mathrm{F}}-k)\right]\Theta(|k+k_{\mathrm{F}}| - \Lambda a_0), \tag{20}$$

the occupation number of momentum k. These relations can be complemented by $n_k = 0$ or $n_k = 1$ away from the range of validity of the low-energy theory, i.e., $|k \pm k_{\mathrm{F}}| > \Lambda a_0$. Figure 2(b) shows n_k for $T_{\mathrm{L}}, T_{\mathrm{R}} = 0$ and for finite but distinct T_{L} and T_{R}. For finite V, there is a double step structure around each Fermi point with width $\Delta = a_0V/v$ and height b_{L} (b_{R}) for k near k_{F} ($-k_{\mathrm{F}}$). A single step per Fermi point is recovered in three different cases: for reflectionless leads, with $b_{\mathrm{L}} = 1, b_{\mathrm{R}} = 0$, reproducing the results obtained using Landauer reservoirs; when one of the leads effectively decouples, $b_{\mathrm{L}} = 1, b_{\mathrm{R}} = 1$ ($b_{\mathrm{L}} = 0, b_{\mathrm{R}} = 0$), i.e., the wire coupling to the left (right) lead is much larger than that of the right (left), in which case the wire distribution function becomes that of the lead which strongly couples to the system. The steps are smoothened with the temperature associated to the respective reservoir. For $T_{\mathrm{L}}, T_{\mathrm{R}} \neq 0$, $\varrho_r \propto e^{-|r|/\xi}$ decays exponentially in r, with a temperature-dependent characteristic length ξ that diverges as T_{L} or T_{R} vanish. For $T_{\mathrm{L}}, T_{\mathrm{R}} = 0$, one obtains $\varrho_r =$

$\frac{1}{r}\{\sin(\frac{\Delta r}{2})[(b_L-1)e^{-irk_F}+b_R e^{irk_F}]+e^{-\frac{1}{2}i\Delta r}\sin(rk_F)\}$, corresponding to a $1/r$ decay as in the equilibrium $T=0$ case. For reflectionless leads, i.e., $b_L=1$, $b_R=0$, the argument of ϱ_r becomes linear in r: $\arg(\varrho_r)=-\frac{1}{2}\Delta r$, as observed in the CCSS formed after a quench in Refs. [26,28]. The local distribution function, as measured by tunneling spectroscopy, is $n_{\rm local}(\omega)=[n_R(\omega)+n_L(\omega)]/2$, which, for equal contacts (i.e., $b_L+b_R=1$), becomes independent of b_l. Tunneling spectroscopy measurements performed with similar contacts can therefore be insensitive to some of the features of n_k. The particle current $J=-it\langle c_r^\dagger c_{r+1}-c_{r+1}^\dagger c_r\rangle$, given in the low-energy sector by $J\simeq\frac{1}{2\pi}(b_L-b_R)V$, is independent of v and of the temperature, assuming for consistency $\Delta\ll 1$.

In addition to static quantities, the CCSS is characterized by its dynamic correlators. Figure 2(a) depicts the one point function $\mathcal{J}_k(\omega)=-i\frac{1}{2\pi}G_k^<(\omega)=\frac{1}{2}[\rho_k^-(\omega)-\rho_k^+(\omega)]$ that is proportional to the transition rate as measured by angle-resolved photoemission spectroscopy. For $|\omega|<\Lambda v$, it can be approximated by $\mathcal{J}_k(\omega)\simeq n_k\{\delta[\omega-va_0^{-1}(k-k_F)]+\delta[\omega+va_0^{-1}(k+k_F)]\}$, thus the step structure of Fig. 2(a) is the same as n_k. Even at zero temperature, there is a nonvanishing probability of finding a particle above ε_F for $V>0$ and thus $\mathcal{J}_k(\omega>0)$ does not vanish.

B. Particle-number fluctuations and entanglement entropy

We now turn to the characterization of the CCSS in terms of its particle-number fluctuations and entanglement content. For the equilibrium ground state of a Fermi gas, i.e., at $T=0$, both the second moment of the distribution of the number of particles in a subregion and its entanglement entropy scale as the logarithm of the subregion size ℓ with universal prefactors [44–47]. For finite temperatures, this behavior is observed for $\ell\ll v/T$ above which it crosses over to an extensive dependence in ℓ. In this section, we study these quantities in the presence of nonequilibrium conditions imposed by the thermodynamic unbalanced leads.

The generating function for the particle-number fluctuations in a region Σ is given by

$$\chi(\lambda)=\sum_m P_m e^{i\lambda m}=\mathrm{tr}(\hat\rho_\Sigma e^{i\lambda N_\Sigma}), \tag{21}$$

where P_m is the probability of finding m particles in region Σ, $N_\Sigma=\sum_{r\in\Sigma}c_r^\dagger c_r$, and $\hat\rho_\Sigma=\mathrm{tr}_{\bar\Sigma}\hat\rho$ is obtained from the total density matrix $\hat\rho$ by tracing out the degrees of freedom belonging to $\bar\Sigma$, the complement of Σ. The fluctuations of the number of particles was shown to be intimately related to the entanglement entropy of a region Σ [44–47], defined as $S_\Sigma=-\mathrm{tr}(\hat\rho_\Sigma\ln\hat\rho_\Sigma)$. In the following, we consider a region Σ_ℓ of size ℓ and denote $S_\ell=S_{\Sigma_\ell}$. Since the model is noninteracting, the entanglement entropy can be obtained from $\varrho_\ell=\sum_{rr'\in\Sigma_\ell}|r\rangle\varrho_{rr'}\langle r|$, with the single-particle density matrix restricted to Σ_ℓ, as $S_\ell=\mathrm{tr}[s(\varrho_\ell)]$, where $s(\nu)=-\nu\ln\nu-(1-\nu)\ln(1-\nu)$. Similarly, using the Levitov-Lesovik determinant formula [48], we arrive at $\chi(\lambda)=\det[1-\varrho_\ell(1-e^{i\lambda})]$. Both quantities can be related to $\det[z-\varrho_\ell]$: the generation function is simply obtained by $\ln\chi(\lambda)=-\ell\ln z+\ln\det[z-\varrho_\ell]$ with $z=(1-e^{i\lambda})^{-1}$, and the entanglement entropy can be written as

$$S_\ell=\frac{1}{2\pi i}\oint dz\, s(\nu)\,\partial_z\ln\det[z-\varrho_\ell], \tag{22}$$

following Ref. [49]. This connection has been explored to relate the entanglement entropy to the fluctuations of the particle number [44–47]. In particular, for the ground state of a gapless one-dimensional system, the second moment $\mathcal{F}_\ell=\langle N_\ell^2\rangle-\langle N_\ell\rangle^2$ was observed to have logarithmic diverging terms in ℓ, i.e., $\mathcal{F}\propto\ln\ell$, whenever they were present for the entanglement entropy [45] in such a way that $S_\ell/\mathcal{F}_\ell=\pi c/(3v\kappa)$, with c the central charge and κ the compressibility. This is particularly interesting since fluctuations can, in principle, be measured experimentally and this connection thus permits the study of the entanglement entropy that suffers from a general lack of measurement methods.

In the case where Σ_ℓ is chosen in the center of the wire and $\ell\ll N$, $D_\ell[\phi]=\det[z-\varrho_\ell]$ becomes a Toplitz determinant, where $\phi(k)=z-n_k$ is called the symbol of the Toplitz matrix $z-\varrho_\ell=\sum_{rr'\in\Sigma_\ell}|r\rangle\int\frac{dk}{2\pi}\phi(k)e^{ik(r-r')}\langle r'|$. $D_\ell[\phi]$ can be computed asymptotically for large values of ℓ using some results for approximating determinants of Toplitz matrices in the $\ell\to\infty$ limit [49]. For $T_R,T_L\neq 0$, the symbol $\phi(k)$ is a smooth function of k, thus the Szegö's limit theorem can be employed yielding $S_\ell=-\ell\sum_l\int_{-\infty}^{\infty}\frac{dk}{2\pi}s[n_k]+\gamma_A$, where γ_A is an ℓ independent constant and $\ln\chi(\lambda)=\ell\int\frac{dk}{2\pi}\ln[1-n_k(1-e^{i\lambda})]+O(\ell^0)$. For the case $T_R,T_L=0$, we have to appeal to the Fisher-Hartwing conjecture for the case of Fig. 2(b) (blue line), where n_k has four discontinuities rather then the two present at equilibrium. Following the same steps as in Ref. [49], detailed in Appendix D, we obtain

$$\ln\chi(\lambda)=\kappa_V\ell+\tilde\kappa_V\ln(\ell)+\kappa_A+O(1/\ell), \tag{23}$$

with κ_A is an ℓ-independent constant,

$$\kappa_V=\left(\frac{2k_F-\Delta}{2\pi}\right)i\lambda+\left(\frac{\Delta}{2\pi}\right)\ln\{[1-b_L(1-e^{i\lambda})]\times[1-b_R(1-e^{i\lambda})]\}, \tag{24}$$

and $\tilde\kappa_V=-\sum_{j=0}^4\beta_j^2$, where β_j are functions of $z=(1-e^{i\lambda})^{-1}$ that also depend on b_L and b_R and are defined in Appendix D. For the second moment, we explicitly obtain

$$\mathcal{F}_\ell=\ell\frac{\Delta[(1-b_L)b_L+(1-b_R)b_R]}{4\pi}+\frac{\ln(\ell)}{2\pi^2}[1-(1-b_L)b_L-(1-b_R)b_R]. \tag{25}$$

This expression reduces to the equilibrium zero-temperature result $\mathcal{F}_\ell=-\frac{\ln(\ell)}{2\pi^2}$ [47] for $b_{R,L}=0,1$. Note that the second term only depends on the number of discontinuities of n_k and their magnitude, having no dependence of Δ. This renders nonanalytic the limit $\Delta\to 0$ since the equilibrium result is not recovered by Eq. (25) at $\Delta=0$.

For the entanglement entropy, after evaluating the contour integral in Eq. (22) (see details in Appendix D), we find

$$S_\ell=\gamma_V\ell+\tilde\gamma_V\ln(\ell)+\gamma_A+O(1/\ell), \tag{26}$$

where γ_A is an ℓ-independent constant, $\gamma_V=\frac{\Delta}{2\pi}[s(b_L)+s(b_R)]$ is the coefficient of the volume term,

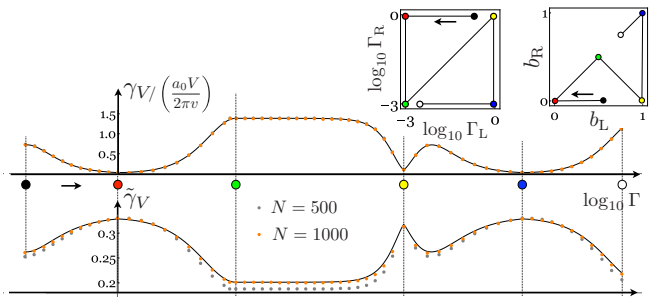

FIG. 3. Extensive coefficient of the entanglement entropy γ_V and logarithmic correction $\tilde{\gamma}_V$ computed for a set of points $\{\Gamma_L,\Gamma_R\}$ following the color code in the inset. The second inset depicts the corresponding $\{b_L,b_R\}$ values. The numerical values obtained for the tight-binding model with $\varepsilon_F = 0.3t$, $V = 0.2t$, and $T_L = T_R = 0$ are compared with the low-energy theory predictions (black line).

and $\tilde{\gamma}_V = \frac{1}{3} - \tilde{s}(b_L) - \tilde{s}(b_R)$ with

$$\tilde{s}(b) = \frac{1}{24} + \frac{1}{4\pi^2}\{(2b-1)[\mathrm{Li}_2(1-b) - \mathrm{Li}_2(b)] + (1-b)\ln^2(1-b) + b\ln^2(b) + \ln(b)\ln(1-b)\},$$

which is the coefficient of the logarithmic correction that is voltage independent. We note that Ref. [50] has considered the calculation of Renyi entropies with discontinuities in n_k of the kind we encounter here, although dealing with an equilibrium setup.

The logarithmic correction is particularly important for the mutual information $S(A,B) = S_A + S_B - S_{A+B}$ between two adjacent segments of length $\ell/2$. Here the volume term cancels and thus $S(A,B) = \tilde{\gamma}_V \ln(\ell) + \gamma_A - 2\tilde{\gamma}_V \ln(2) + O(1/\ell)$, which can be used to directly compute $\tilde{\gamma}_V$ numerically. Figure 3 shows γ_V and $\tilde{\gamma}_V$ as a function of the hybridization along a path in the $\Gamma_L - \Gamma_R$ plane as well as the corresponding values in the $b_L - b_R$ plane. With increasing system size, the numerical results obtained for the tight-binding model converge to the analytic predictions. γ_V and $\tilde{\gamma}_V$ vary in the opposite sense—a large volume term corresponds to a small mutual information content. The maximum value $\tilde{\gamma}_V = 1/3$, obtained at equilibrium, is attained for $V > 0$ whenever b_L and b_R are such that only two discontinuities arise in n_k, in which case $\gamma_V = 0$. Similar to what happens for $\tilde{\kappa}_V$, for a generic point in the $b_L - b_R$ plane with $\tilde{\gamma}_V \neq 1/3$, the limit $V \to 0$ is singular since for $V = 0$, and only at that point, one recovers the equilibrium value $\tilde{\gamma}_V = 1/3$. Figure 4 depicts the ℓ and the $\ln\ell$ coefficients of the entanglement entropy S_ℓ, respectively γ_V and $\tilde{\gamma}_V$, as a function of the voltage. The

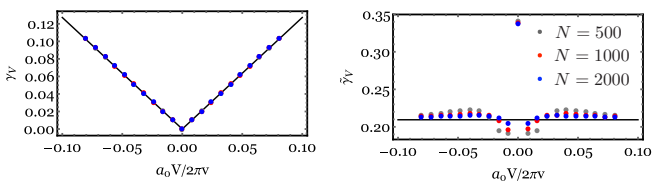

FIG. 4. Volume γ_V and logarithmic $\tilde{\gamma}_V$ coefficients of the entanglement entropy as a function of the applied voltage V computed for $\Gamma_L = 0.02t$, $\Gamma_R = 0.01t$, $\varepsilon_F = 0.3t$, and $T_L = T_R = 0$.

numerical results obtained for the tight-binding model are seen to converge to the analytic curves predicted by the continuum model. We observe that $\gamma_V \propto |V|$ and that $\tilde{\gamma}_V$ is V independent for $V \neq 0$. At $V = 0$, we recover the equilibrium result $\tilde{\gamma}_V = 1/3$. The observed singularity prohibits the calculation of the entanglement entropy and of the number fluctuations perturbatively in V and thus this quantity cannot be obtained from linear response arguments.

C. Two-point correlations

Finally, we analyze the two-point density-density correlations and response functions of the CCSS encoded in the lesser and greater components of the charge susceptibility $\chi^{>}_{rr'}(t,t') = -i\langle \hat{n}_r(t)\hat{n}_{r'}(t')\rangle$, $\chi^{<}_{rr'}(t,t') = -i\langle \hat{n}_{r'}(t')\hat{n}_r(t)\rangle$. As for the one-point function, for r,r' in the central region of the wire, $\chi^{>,<}_{rr'}$ become approximately translationally invariant. In this regime, the Fourier transformed quantities $\chi^{\pm}_p(\nu) = -\frac{1}{2\pi i}[\chi^{>}_p(\nu) \pm \chi^{<}_p(\nu)]$ are given by

$$\chi^{\pm}_p(\nu) = \left[\chi^{\pm}_{\mathrm{LL}}\left(\nu, a_0^{-1}p\right) + \chi^{\pm}_{\mathrm{RR}}\left(\nu, a_0^{-1}p\right)\right] + \chi^{\pm}_{\mathrm{LR}}\left[\nu, a_0^{-1}(p-2k_F)\right] + \chi^{\pm}_{\mathrm{RL}}\left[\nu, a_0^{-1}(p+2k_F)\right], \tag{27}$$

where the first two terms correspond to low momentum ($|p| < a_0\Lambda$) and the last two terms to $2k_F$ contributions ($|p-2k_F| < a_0\Lambda$ and $|p-2k_F| < a_0\Lambda$) and where

$$\chi^{+}_{ll}(\nu q) = \frac{1}{2v}\delta(\nu \mp vq)\int \frac{d\omega}{2\pi}[1 - F_l(\omega)F_l(\omega-\nu)],$$
$$\chi^{+}_{l\bar{l}}(\nu q) = \frac{1}{4\pi v}\left[1 - F_l\left(\frac{\pm vq+\nu}{2}\right)F_{\bar{l}}\left(\frac{\pm vq-\nu}{2}\right)\right],$$
$$\chi^{-}_{ll}(\nu q) = \frac{1}{2v}\delta(\nu \mp vq)\int \frac{d\omega}{2\pi}[F_l(\omega) - F_l(\omega-\nu)],$$
$$\chi^{-}_{l\bar{l}}(\nu q) = \frac{1}{4\pi v}\left[F_l\left(\frac{\pm vq+\nu}{2}\right) - F_{\bar{l}}\left(\frac{\pm vq-\nu}{2}\right)\right], \tag{28}$$

where the upper (lower) signs are for $l = R$ ($l = L$) and $F_l(\omega) = 1 - 2n_l(\omega)$. The details of the calculation are provided in Appendix E. The dynamical structure factor $S_p(\nu) = i\chi^{>}_p(\nu)$, that can be directly accessed by neutron scattering is shown is Fig. 5 for $T_L = T_R = 0$. As in equilibrium, the contribution at low momentum is coherent, but the δ-function

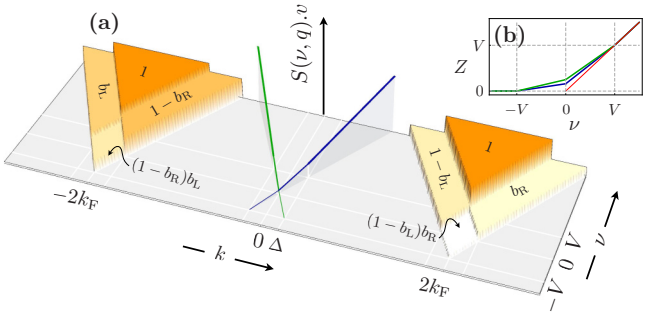

FIG. 5. (a) Dynamical structure factor $S_p(\nu) = i\chi^{>}_p(\nu)$, directly accessible by neutron scattering. (b) Weight of the δ-function Z for the positive (blue) and negative (green) velocity branches near $k = 0$. The red line depicts the equilibrium, i.e., $V = 0$, result.

weight Z acquires a nontrivial dependence on frequency, as seen in the inset. Contributions near $\pm k_F$ form the particle-hole excitation continuum and also develop a steplike structure dependent on b_L and b_R that gets smeared out at finite temperatures. In the reflectionless case $b_L = 1, b_R = 0$, the particle-hole continuum is simply shifted up (down) in energy for positive (negative) momentum.

V. DISCUSSION

The properties of a CCSS in the bulk of a thermodynamically unbalanced one-dimensional system are found to crucially depend on the couplings to the leads which induce a double-step momentum occupation number near each Fermi point. This feature imprints a clear signature to the one- and two-point functions, as depicted in Figs. 2(a) and 5. As in equilibrium, the structure factor consists of a coherent branch around zero momentum and a quasiparticle continuum around $\pm 2k_F$. Besides an abrupt change of the weight of the coherent excitation for energies corresponding to plus or minus the bias voltage, nonequilibrium conditions lead to a set of steps in the incoherent component. In frequency, the steps arise at the energy of the applied bias voltage, while in momentum they are observed for momenta that differ from $\pm 2k_F$ by the bias voltage divided by the Fermi velocity. The height of the steps is set by the couplings to the contacts and can be interpreted within a Landauer-like scattering approach by considering imperfect contacts with a finite reflection coefficient. In the reflectionless case, corresponding to ideal Landauer contacts, the asymmetry between the $\pm 2k_F$ components can be simply linked to the energy difference between the Fermi surfaces of the right and left reservoirs.

The experimental detection of these features requires probes that can resolve both momentum and energy and a clean system in the ballistic regime. In equilibrium, the one-point function in quasi-one-dimensional organic conductors can be accessed by angle-resolved photoemission spectroscopy (ARPES) [51–53]. By contacting the sample to external leads, such setup could in principle be used to access the nonequilibrium spectral function and detect the double step depicted in Fig. 2(a). In solid-state setups, the equilibrium structure factor is accessible by neutron scattering. While for insulating quasi-one-dimensional materials this technique has been extensively employed to study magnetic excitations [54,55], in the absence of a charge gap its use has been more challenging [56–58]; nonetheless this technique can as well be used to probe the structure factor away from equilibrium. Momentum-resolved studies of one-dimensional systems are also available in cold-atomic setups [59–61] where the dynamic structure factor can be probed by Bragg spectroscopy [62]. While for the moment the reported transport setups [63] are restricted to point contacts between reservoirs, their versatility could in the near future allow for the investigation of extended one-dimensional systems.

One-dimensional electronic systems are strongly affected by electron-electron interactions; therefore, it is natural to wonder about the stability and relevance of the predictions above, obtained in the strict noninteracting limit. For a Luttinger liquid at equilibrium, the Fermi-step discontinuity observed in the noninteracting momentum distribution function is smeared out. On the other hand, the dynamical one- and two-point functions are characterized by a set of power laws near spectral edges [56,64–69]. For the out-of-equilibrium reflectionless case, since in one dimension kinetic constraints ensure that relaxation can be neglected at low energies, the distribution function of left (right) movers is solely fixed by the right (left) reservoir, even in the presence of interactions. This was investigated in Refs. [12–17] . Even though, to our knowledge, the nonequilibrium momentum- and energy-resolved response functions have not been studied, the techniques therein could be used to obtain response functions in the presence of interactions. In this case, one expects the set of nonequilibrium spectral edges reported here for the noninteracting case to acquire the power-law features at the spectral edges characteristic of Luttinger liquids.

Let us now discuss the results regarding the entanglement properties. The direct measurement of entanglement entropy of a subregion remains a challenge; however, it is possible to access some of its signatures by monitoring the fluctuations of the number of particles within the same volume. Such measurements are naturally available for quantum point contacts and in cold-atomic setups by procedures that are extendable to the nonequilibrium regime.

For a generic CCSS, the entanglement entropy and the second moment of the particle-number fluctuations are found to be proportional to the volume of the system and to the applied voltage, even at zero temperature. For the entropy, the prefactor of the extensive contribution is simply the free-fermion entropy computed from the momentum distribution function. As in equilibrium, there is a zero-temperature subextensive contribution that goes as the logarithm of the system size. The existence of an extensive zero-temperature contribution to S_ℓ and $\mathcal{F}_\ell$, for $V \neq 0$ and $b_L, b_R \neq 0, 1$, makes the generic nonequilibrium case quite different from the equilibrium one, where $S_\ell/\mathcal{F}_\ell$ was found to simply depend only on the ratio $c/(\kappa v)$. Nonetheless, the knowledge of the moments of the number-fluctuation distribution permits one to reconstruct the entanglement entropy [46] and can thus be used as a means to measure this quantity in a CCSS. As in equilibrium, the logarithmic contribution seen at zero temperature can be observed for system sizes $\ell \ll v/T$, above which there is a crossover to the purely extensive behavior observed at finite temperatures.

As a consequence of the subextensive term appearing in the entanglement entropy, the mutual information of two adjacent segments grows logarithmically with the segment length. Interestingly, the prefactor differs from the equilibrium in a singular way: it is $1/3$ for the equilibrium $V = 0$ case and, for $|V| > 0$, it is a voltage-independent function of the contact properties. This implies that the equilibrium result, which can be obtained by conformal field theory arguments for gapless one-dimensional phases with unit central charge, does not hold away from equilibrium. The particular functional form of the logarithmic prefactor of the mutual information of two adjacent segments shows that their shared information is never larger than at equilibrium and that a steady-state current thought the system cannot carry any additional information between the segments. A similar modification of the area-law violation for the mutual information has been observed in the CCSS formed after a quench of two chains at different

temperatures [37]. In this case, the discontinuity in the momentum distribution arises at $k = 0$ and π, for energies where the dispersion relation is not linear; thus it depends on the details of the band structure and cannot be captured by the low-energy description used in this work. Modifications to the equilibrium area-law violation suggest that the physics away from equilibrium may be ruled by low-energy fixed-point theories fundamentally different from the equilibrium ones.

ACKNOWLEDGMENTS

We gratefully acknowledge discussions with D. Esteve, M. Haque, S. Kirchner, A. Lazarides, A. Rubtsov, P. Sacramento, and V. R. Vieira. P.R. acknowledges support by FCT through the Investigador FCT Contract No. IF/00347/2014 and Grant No. UID/CTM/04540/2013.

APPENDIX A: IDENTIFICATIONS WITH THE TIGHT-BINDING MODEL I: GREEN'S FUNCTIONS

Using that, in the low-energy sector, $c_r \simeq e^{ik_F r}\psi_L(a_0 r) + e^{-ik_F r}\psi_R(a_0 r)$, the Green's function of the tight-binding model on the Keldysh contour can be approximated by

$$\begin{aligned} G_{rr'}(z,z') &\equiv -i\langle T_\gamma c_r(z)\cdot c^\dagger_{r'}(z')\rangle \\ &\simeq (e^{ik_F r}\ \ e^{-ik_F r})\cdot \boldsymbol{G}\big(zra_0^{-1}, z'r'a_0^{-1}\big)\cdot \begin{pmatrix} e^{-ik_F r'} \\ e^{ik_F r'}\end{pmatrix}, \end{aligned} \tag{A1}$$

where

$$\boldsymbol{G}(zx,z'x') \equiv -i\langle T_\gamma \Psi(zx)\cdot \Psi^\dagger(z'x')\rangle \tag{A2}$$

is the continuum Green's function and T_γ is the time-ordered operator for two times z and z' on the Keldysh contour γ. We use the standard definitions of larger and lesser Green's functions, $\boldsymbol{G}^{>(<)}(tx,t'x') \equiv \boldsymbol{G}(tx,t'x')$, for $z = t$ $(z' = t')$ coming after $z' = t'$ $(z = t)$ along γ, and

$$\begin{aligned} \mathbf{G}^R(tx,t'x') &\equiv \Theta(t-t')[\mathbf{G}^>(tx,t'x') - \mathbf{G}^<(tx,t'x')], \\ \mathbf{G}^A(tx,t'x') &\equiv -\Theta(t'-t)[\mathbf{G}^>(tx,t'x') - \mathbf{G}^<(tx,t'x')], \\ \mathbf{G}^K(tx,t'x') &\equiv \mathbf{G}^>(tx,t'x') + \mathbf{G}^<(tx,t'x'). \end{aligned} \tag{A3}$$

We use the notation $\mathbf{G}^a(tx,t'x') = \langle x|\mathbf{G}^a(t,t')|x'\rangle$, for $a = R,A,K$, and in the steady state we define $\boldsymbol{G}^a(\omega) = \int \frac{d\omega}{2\pi} e^{i\omega(t-t')}\boldsymbol{G}^a(t,t')$. For convenience, we work with the quantities

$$\boldsymbol{\rho}^-(\omega) = -[\boldsymbol{G}^R(\omega) - \boldsymbol{G}^A(\omega)]/(2\pi i), \tag{A4}$$

$$\boldsymbol{\rho}^+(\omega) = -\boldsymbol{G}^K(\omega)/(2\pi i), \tag{A5}$$

rather than the Green's functions themselves. These are proportional to the spectral function and to the imaginary part of the Keldysh Green's function, respectively, and encode the same physical information. Note that defined in this way, both $\rho^\pm$ are Hermitian matrices $(\rho^\pm)^\dagger = \rho^\pm$. As in Eq. (A1), we also have the relation

$$\rho^\pm_{rr'}(\omega) \simeq (e^{ik_F r}\ \ e^{-ik_F r})\cdot \boldsymbol{\rho}^\pm\big(\omega; ra_0^{-1}, r'a_0^{-1}\big)\cdot \begin{pmatrix} e^{-ik_F r'} \\ e^{ik_F r'}\end{pmatrix} \tag{A6}$$

between continuum and tight-binding quantities.

APPENDIX B: EXPLICIT EXPRESSIONS FOR THE GREEN'S FUNCTIONS

1. Retarded and advanced Green's functions

Using the previously obtained eigensystem of K, the retarded and advanced components of the Green's function for $x,x' \in I_0$ are given by

$$\begin{aligned} \langle x|\boldsymbol{G}^R(\omega)|x'\rangle = \frac{1}{2L}\sum_n \begin{pmatrix} e^{i\phi_L}e^{-2a\gamma_L}e^{iq_n x} \\ e^{-iq_n x}\end{pmatrix}\frac{1}{\omega - vq_n} \\ \times (e^{-i\phi_L}e^{2a\gamma_L}e^{-iq_n x'}\ \ e^{iq_n x'}) \end{aligned} \tag{B1}$$

and $\boldsymbol{G}^A(\omega) = [\boldsymbol{G}^R(\omega)]^\dagger$. The sum over the quantized q_n's can be replaced by the contour integral,

$$\begin{aligned} \frac{1}{2L}\sum_n \frac{e^{iq_n x}}{\omega - vq_n} &= \oint_{z_i}\frac{dq}{2\pi}\frac{e^{iq_n x}}{\omega - vq_n} z_\pm(q) \\ &= \frac{i}{v} z_\pm(\omega v^{-1}) e^{i\omega v^{-1}x}, \end{aligned} \tag{B2}$$

where

$$z_\pm(q) = \frac{\pm 1}{e^{\pm[2iqL - 2a(\gamma_L+\gamma_R)+i(\phi_L-\phi_R)]} - 1}, \tag{B3}$$

for $x > 0$ or $x < 0$, respectively, can be chosen in order to render the integral convergent once the contour is deformed. Using this identity, we obtain

$$\begin{aligned} \langle x|\boldsymbol{\rho}^-(\omega)|x'\rangle = \frac{1}{2\pi v}\frac{\sinh(2a\gamma_L)}{\sinh[2a(\gamma_L+\gamma_R)]}\begin{pmatrix} e^{2a\gamma_R}u_{L,0}(\omega v^{-1})e^{i\omega v^{-1}(x-x')} & e^{i\phi_L}u_{L,-2}(\omega v^{-1})e^{i\omega v^{-1}(x+x')} \\ e^{-i\phi_L}u_{L,2}(\omega v^{-1})e^{-i\omega v^{-1}(x+x')} & e^{-2a\gamma_R}u_{L,0}(\omega v^{-1})e^{-i\omega v^{-1}(x-x')}\end{pmatrix} \\ + \frac{1}{2\pi v}\frac{\sinh(2a\gamma_R)}{\sinh[2a(\gamma_L+\gamma_R)]}\begin{pmatrix} e^{-2a\gamma_L}u_{L,0}(\omega v^{-1})e^{i\omega v^{-1}(x-x')} & e^{i\phi_L}u_{L,0}(\omega v^{-1})e^{i\omega v^{-1}(x+x')} \\ e^{-i\phi_L}u_{L,0}(\omega v^{-1})e^{-i\omega v^{-1}(x+x')} & e^{2a\gamma_L}u_{L,0}(\omega v^{-1})e^{-i\omega v^{-1}(x-x')}\end{pmatrix} \end{aligned} \tag{B4}$$

where we defined

$$u_{L,n}(q) = -\frac{e^{i[qL+\frac{1}{2}(\phi_L-\phi_R)]n}\sinh[2a(\gamma_L+\gamma_R)]}{\cos[2qL+(\phi_L-\phi_R)] - \cosh[2a(\gamma_L+\gamma_R)]}. \tag{B5}$$

In the limit $L \to \infty$, one has that for a regular function $f(q)$ and $\epsilon > 0$ independent of L,

$$\lim_{L\to\infty} \frac{1}{2\epsilon} \int_{q-\epsilon}^{q+\epsilon} dq'\, u_{L,n}(q') f(q') = u_n\ f(q), \tag{B6}$$

with

$$u_0 = u_{\pm 2} 1; \quad u_{\pm 1} = 0 := e^{-2a(\gamma_L+\gamma_R).} \tag{B7}$$

Using these limiting identities, for $|x|, |x'| \ll L/2$ and $L \to \infty$, the spectral function in the middle of the wire is given by

$$\langle x|\boldsymbol{\rho}^-_{\text{bulk}}(\omega)|x'\rangle \equiv \langle x + L/2|\boldsymbol{\rho}^-(\omega)|x' + L/2\rangle = \frac{1}{2\pi v}\begin{pmatrix} e^{i\omega v^{-1}(x-x')} & 0 \\ 0 & e^{-i\omega v^{-1}(x-x')} \end{pmatrix}. \tag{B8}$$

2. Keldysh Green's functions

In the steady state, the Keldysh component of the Green's function is given by $G^K = G^R \Sigma^K G^A$ with $\Sigma^K = \Sigma^K_L + \Sigma^K_R$ and

$$\langle x|\boldsymbol{\Sigma}^K_l(\omega)|x'\rangle = -2i v\, \gamma_l \Theta(|x - x_l| - a)\delta(x - x') \tanh\left[\frac{\beta_l}{2}(\omega - \mu_l)\right]\sigma_0, \tag{B9}$$

which yields

$$\langle x|\boldsymbol{G}^K(\omega)|x'\rangle = \sum_{l=L,R} \int_{I_l} dy\, \langle x|\boldsymbol{G}^R(\omega)|y\rangle \langle y|\boldsymbol{\Sigma}^K_l(\omega)|y\rangle \langle y|\boldsymbol{G}^A(\omega)|x'\rangle. \tag{B10}$$

For $x, x' \in I_0$, one gets

$$\begin{aligned}\langle x|\boldsymbol{\rho}^+(\omega)|x'\rangle = {} & \frac{1}{2\pi v} \tanh\left[\frac{\beta_L}{2}(\omega - \mu_L)\right] \frac{\sinh(2a\gamma_L)}{\sinh[2a(\gamma_L+\gamma_R)]} \begin{pmatrix} e^{2a\gamma_R} u_{L,0}(\omega v^{-1}) e^{i\omega v^{-1}(x-x')} & u_{L,-2}(\omega v^{-1}) e^{i\phi_L} e^{i\omega v^{-1}(x+x')} \\ u_{L,2}(\omega v^{-1}) e^{-i\phi_L} e^{-i\omega v^{-1}(x+x')} & e^{-2a\gamma_R} u_{L,0}(\omega v^{-1}) e^{-i\omega v^{-1}(x-x')} \end{pmatrix} \\ & + \frac{1}{2\pi v} \tanh\left[\frac{\beta_R}{2}(\omega - \mu_R)\right] \frac{\sinh(2a\gamma_R)}{\sinh[2a(\gamma_L+\gamma_R)]} \begin{pmatrix} u_{L,0}(\omega v^{-1}) e^{-2a\gamma_L} e^{i\omega v^{-1}(x-x')} & u_{L,0}(\omega v^{-1}) e^{i\phi_L} e^{i\omega v^{-1}(x+x')} \\ e^{-i\phi_L} u_{L,0}(\omega v^{-1}) e^{-i\omega v^{-1}(x+x')} & e^{2a\gamma_L} u_{L,0}(\omega v^{-1}) e^{-i\omega v^{-1}(x-x')} \end{pmatrix}. \end{aligned} \tag{B11}$$

As before, for $|x|, |x'| \ll L/2$ and $L \to \infty$, we obtain

$$\begin{aligned}\langle x|\boldsymbol{\rho}^+_{\text{bulk}}(\omega)|x'\rangle \equiv {} & \langle x + L/2|\boldsymbol{\rho}^+(\omega)|x' + L/2\rangle \\ = {} & \frac{1}{2\pi v} \tanh\left[\frac{\beta_L}{2}(\omega - \mu_L)\right] \frac{\sinh(2a\gamma_L)}{\sinh[2a(\gamma_L+\gamma_R)]} \begin{pmatrix} e^{2a\gamma_R} e^{i\omega v^{-1}(x-x')} & 0 \\ 0 & e^{-2a\gamma_R} e^{-i\omega v^{-1}(x-x')} \end{pmatrix} \\ & + \frac{1}{2\pi v} \tanh\left[\frac{\beta_R}{2}(\omega - \mu_R)\right] \frac{\sinh(2a\gamma_R)}{\sinh[2a(\gamma_L+\gamma_R)]} \begin{pmatrix} e^{-2a\gamma_L} e^{i\omega v^{-1}(x-x')} & 0 \\ 0 & e^{2a\gamma_L} e^{-i\omega v^{-1}(x-x')} \end{pmatrix}. \end{aligned}$$

APPENDIX C: IDENTIFICATIONS WITH THE TIGHT-BINDING MODEL II: ϕ_l AND γ_l

1. Determination of ϕ_l

The tight-binding Hamiltonian, given by

$$\boldsymbol{H}_{\text{TB}} = -t\left[\left(\sum_{r=0}^{N-2} |r\rangle\langle r+1|\right) + \text{H.c.}\right], \tag{C1}$$

has wave functions of the form

$$\psi(r) = \langle r\,|\psi_k\rangle = Ae^{ikr} + Be^{-ikr}, \tag{C2}$$

and the dispersion relation

$$\varepsilon_k = -2\cos(k). \tag{C3}$$

The quantization condition for the momentum can be obtained imposing $\langle r = 0|\boldsymbol{H}_{\text{TB}}|\psi_k\rangle = \varepsilon_k\langle 0|\psi_k\rangle$ and $\langle r = N-1|\boldsymbol{H}_{\text{TB}}|\psi_k\rangle = \varepsilon_k\langle N-1|\psi_k\rangle$ and are equivalent to the relations

$$\psi(-1) = \psi(N) = 0. \tag{C4}$$

For the wave function expanded around k_F,

$$\langle r|\psi_k\rangle \simeq e^{ik_F r}\langle x = a_0 r|\psi_L\rangle + e^{-ik_F r}\langle x = a_0 r|\psi_R\rangle, \tag{C5}$$

this implies, in the limit $a_0 \to 0$, $a_0 N \to L$,

$$e^{-ik_F}\langle 0|\psi_L\rangle + e^{ik_F r}\langle 0|\psi_R\rangle = 0, \tag{C6}$$

$$e^{ik_F L a_0^{-1}}\langle L|\psi_L\rangle + e^{-ik_F L a_0^{-1}}\langle L|\psi_R\rangle = 0, \tag{C7}$$

yielding to the phase shifts

$$\phi_L = 2k_F - \pi, \tag{C8}$$

$$\phi_R = -2k_F L a_0^{-1} - \pi. \tag{C9}$$

2. Determination of γ_l

The eigenvectors of the tight-binding version of the $\boldsymbol{K}$ operator,

$$\boldsymbol{K}_{\rm TB} = -t\left[\left(\sum_{r=1}^{N-1}|r\rangle\langle r+1|\right)+{\rm H.c.}\right] - i(\Gamma_{\rm L}|1\rangle\langle 1| + \Gamma_{\rm R}|N\rangle\langle N|),$$

can be given in terms of a sum of plane waves and can be obtained in a similar way to that employed in the previous section. The spectrum of $\boldsymbol{K}_{\rm TB}$ is obtained imposing $\langle r=0|\boldsymbol{H}_{\rm TB}|\psi_k\rangle = \varepsilon_k\langle 0|\psi_k\rangle$ and $\langle r=N-1|\boldsymbol{H}_{\rm TB}|\psi_k\rangle = \varepsilon_k\langle N-1|\psi_k\rangle$, and yields

$$\left[\frac{te^{-ik}-i\Gamma_{\rm L}}{te^{ik}-i\Gamma_{\rm L}}\right]\left[\frac{te^{-ik}-i\Gamma_{\rm R}}{te^{ik}-i\Gamma_{\rm R}}\right] = e^{2ikN}.$$

Assuming $k = k_0 + \frac{\Delta k}{N}$, where k_0 is a solution of the equation

$$e^{-4ik_0} = e^{2ik_0N}, \tag{C10}$$

i..e.,

$$k_0 = \frac{\pi}{L+1}n, \tag{C11}$$

and Δk is of the order of $1/N$, we obtain

$$\Delta k = \frac{1}{2}\tan^{-1}\left\{\frac{\sin(2k_0)\left[\left(\Gamma_{\rm R}^2+\Gamma_{\rm L}^2\right)+2\cos(2k_0)\Gamma_{\rm L}^2\Gamma_{\rm R}^2\right]}{\Gamma_{\rm L}^2\Gamma_{\rm R}^2\cos(4k_0)+\left(\Gamma_{\rm L}^2+\Gamma_{\rm R}^2\right)\cos(2k_0)+t^2}\right\} + \frac{1}{4}i\left[\ln\left(-\frac{\Gamma_{\rm L}^2t^{-2}-2t^{-1}\sin k_0\Gamma_{\rm L}+1}{\Gamma_{\rm L}^2t^{-2}+2t^{-1}\sin k_0\Gamma_{\rm L}+1}\right) + \ln\left(-\frac{\Gamma_{\rm R}^2t^{-2}-2t^{-1}\sin k_0\Gamma_{\rm R}+1}{\Gamma_{\rm R}^2t^{-2}+2t^{-1}\sin k_0\Gamma_{\rm R}+1}\right)\right]. \tag{C12}$$

Therefore, near $k_0 = k_{\rm F}$, we get

$$\begin{aligned}{\rm Im}q &= a_0^{-1}{\rm Im}(k_0-k_{\rm F})\\ &= -\frac{1}{4}i\frac{1}{a_0N}\left[\ln\left(-\frac{\Gamma_{\rm L}^2t^{-2}+2t^{-1}\sin k_{\rm F}\Gamma_{\rm L}+1}{\Gamma_{\rm L}^2t^{-2}-2t^{-1}\sin k_{\rm F}\Gamma_{\rm L}+1}\right) + \ln\left(-\frac{\Gamma_{\rm R}^2t^{-2}+2t^{-1}\sin k_{\rm F}\Gamma_{\rm R}+1}{\Gamma_{\rm R}^2t^{-2}-2t^{-1}\sin k_{\rm F}\Gamma_{\rm R}+1}\right)\right].\end{aligned} \tag{C13}$$

Identifying this expression with the quantization condition of the continuum model, we obtain

$$a\gamma_l = \frac{1}{4}\ln\left(-\frac{\Gamma_l^2t^{-2}-2t^{-1}\sin k_{\rm F}\Gamma_l+1}{\Gamma_l^2t^{-2}+2t^{-1}\sin k_{\rm F}\Gamma_l+1}\right), \tag{C14}$$

which for $\Gamma_l \ll 1$ can be approximated by $a\gamma_l \simeq \sin k_{\rm F}\Gamma_l$.

3. Numerical results for the two-point function

Figure 6 shows the one-point functions $\rho^{\pm}_{rr'}(\omega)$ as a function of ω for a finite system. The sharp features with frequency are signatures of the discrete spectrum of the finite chain in the absence of the leads and, in the spectral function $\rho^{-}_{rr'}(\omega)$, they become δ functions in the limit $\Gamma_{\rm L},\Gamma_{\rm R}\to 0$. The infinite volume approximation washes out the rapid variations by averaging over small energy window of the order of the level spacing before taking the $L\to\infty$ limit; see Eq. (B6).

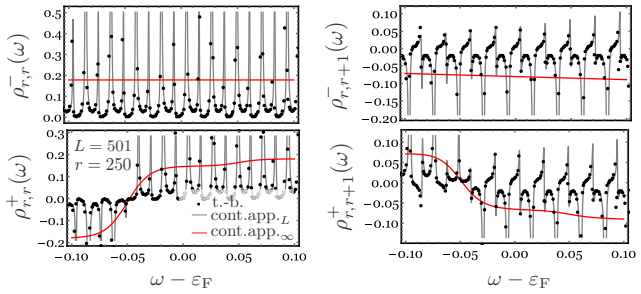

FIG. 6. One-point functions $\rho^{\pm}_{rr'}(\omega)$ as a function of ω computed for $r' = r$ (left panel) and $r' = r+1$ (right panel) and for $r = 250$, $L = 501$, $\Gamma_{\rm L} = 0.5t$, $\Gamma_{\rm R} = 0.2t$, $\varepsilon_{\rm F} = 0.9t$, $V = 0.1t$, and $T_{\rm L} = T_{\rm R} = 0.01t$. The black dots are obtained numerically using the tight-binding model. The black curves are obtained from the continuum limit for finite L using Eqs. (B4) and (B11).

APPENDIX D: CALCULATION OF THE DETERMINANT AND ENTANGLEMENT ENTROPY

For zero temperature, the symbol ϕ is not a smooth function of k. In this case, the Fisher-Hartwing conjecture [49] states that if we decompose the symbol as

$$\phi(\theta) = e^{V(\theta)}e^{i\sum_{i=0}^{m}\beta_i(\theta-\theta_i)}e^{-\pi\sum_{i=0}^{m}\beta_i{\rm sgn}(\theta-\theta_i)} \times\left|2\sin\left(\frac{\theta-\theta_i}{2}\right)\right|^{2\alpha_j}, \tag{D1}$$

where the θ_i's are the points where $\phi(\theta)$ is nonanalytic, α_i and β_i are constants that characterize the nonanalyticities, and $V(\theta)$ is a smooth function of θ, the asymptotic large-ℓ form of the determinant of the Toplitz matrix is given by

$$D_\ell[\phi] \simeq E_{\rm FH}[\phi]e^{\ell V_0+\ln(\ell)\sum_{j=0}^{m}(\alpha_j^2-\beta_j^2)}, \tag{D2}$$

with $E_{\rm FH}[\phi]$ an ℓ-independent constant and

$$V_0 = \int\frac{d\theta}{2\pi}V(\theta).$$

For $T_{\rm R},T_{\rm L} = 0$, the momentum distribution function in the middle of the wire is given by

$$n_k \simeq \begin{cases}1 & -k_{\rm F}+\frac{\Delta}{2} < k < k_{\rm F}-\frac{\Delta}{2}\\ b_{\rm L} & k_{\rm F}-\frac{\Delta}{2} < k < k_{\rm F}+\frac{\Delta}{2}\\ 0 & k_{\rm F}+\frac{\Delta}{2} < k \vee k < -k_{\rm F}-\frac{\Delta}{2}\\ b_{\rm R} & \text{for } -k_{\rm F}-\frac{\Delta}{2} < k < -k_{\rm F}+\frac{\Delta}{2}.\end{cases} \tag{D3}$$

Therefore, decomposing $\phi(\theta) = z - n_\theta$, we obtain

$$\theta_0 = 0;\quad \theta_1 = k_{\rm F}-\frac{\Delta}{2},\quad \theta_2 = k_{\rm F}+\frac{\Delta}{2}, \tag{D4}$$

$$\theta_3 = 2\pi - k_{\rm F}-\frac{\Delta}{2},\quad \theta_4 = 2\pi - k_{\rm F}+\frac{\Delta}{2}, \tag{D5}$$

$\alpha_i = 0$,

$$\beta_0 = 0, \tag{D6}$$

$$\beta_1 = \frac{1}{2\pi i}[\ln(z-1)-\ln(z-b_{\rm R})], \tag{D7}$$

$$\beta_2 = \frac{i}{2\pi}[\ln(z - b_R) - \ln(z)], \tag{D8}$$

$$\beta_3 = \frac{1}{2\pi i}[\ln(z) - \ln(z - b_L)], \tag{D9}$$

$$\beta_4 = \frac{1}{2\pi i}[\ln(z - b_L) - \ln(z - 1)], \tag{D10}$$

and

$$e^{V(\theta)} = (z-1)^{\frac{2k_F-\Delta}{2\pi}} z^{\frac{-\Delta-2k_F+2\pi}{2\pi}} \times (z - b_L)^{\frac{\Delta}{2\pi}} (z - b_R)^{\frac{\Delta}{2\pi}}. \tag{D11}$$

Equation (23) follows immediately from these definitions, given by Eq. (D2), and by setting $z = (1 - e^{i\lambda})^{-1}$. The entanglement entropy is given by

$$S_\ell = \ell\left[\frac{1}{2\pi i}\oint dz\, s(z)\partial_z V_0\right] + \ln(\ell)\left[\frac{1}{2\pi i}\oint dz\, s(z)\,\partial_z \sum_{j=0}^{m}\left(\alpha_j^2 - \beta_j^2\right)\right], \tag{D12}$$

where the contour of integration in Eq. (D12) contains the segment $z \in [0,1]$. Performing the integration explicitly yields Eq. (26).

APPENDIX E: CALCULATION OF THE TWO-PARTICLE CORRELATION FUNCTIONS

The charge susceptibility on the Keldysh contour γ is defined as

$$\chi(zr,z'r') = -i[\langle T_\gamma c_r^\dagger(z^+)c_r(z)c_{r'}^\dagger(z'^+)c_{r'}(z')\rangle - \langle T_\gamma c_r^\dagger(z^+)c_r(z)\rangle\langle T_\gamma c_{r'}^\dagger(z'^+)c_{r'}(z')\rangle], \tag{E1}$$

where the z^+ denotes a point coming infinitesimally later than z along γ. Due to the Gaussian nature of the model,

$$\chi(zr,z'r') = -i\,G_{r'r}(z',z)G_{rr'}(z',z). \tag{E2}$$

The greater and lesser components are given by $\chi^{>,<}(t\boldsymbol{r},t'\boldsymbol{r}') = \chi(z = t\boldsymbol{r}, z' = t'\boldsymbol{r}')$ with z, respectively, after or before z'. For the r and r' in the middle of the wire, using the approximated translationally invariant Green's functions, we obtain

$$\chi_{r,r'}^{>,<}(t,t') = -i[G_L^{<,>}(t'x',tx)G_L^{>,<}(tx,t'x') + G_R^{<,>}(t'x',tx)G_R^{>,<}(tx,t'x') + G_L^{<,>}(t'x',tx)G_R^{>,<}(tx,t'x')e^{-i2k_F(r-r')} + G_R^{<,>}(t'x',tx)G_L^{>,<}(tx,t'x')e^{i2k_F(r-r')}], \tag{E3}$$

with $x = ra_0$, $x' = r'a_0$ and $G_l(zx,z'x') = -i\langle T_\gamma \psi_l(zx)\psi_l^\dagger(zx)\rangle$, since the cross terms $\langle T_\gamma \psi_R(zx)\psi_L^\dagger(zx)\rangle$ vanish. Defining

$$G_l^a(tx,t'x') = \int\frac{d\omega}{2\pi}\int\frac{dq}{2\pi}e^{-i\omega(t-t')}e^{iq(x-x')}G_l^a(\omega k), \tag{E4}$$

we have that for the quantities $\chi_p^\pm(\nu) = -\frac{1}{2\pi i}[\chi_p^>(\nu) \pm \chi_p^<(\nu)]$,

$$\chi_p^\pm(\nu) = \chi_{LL}^\pm\left(\nu,a_0^{-1}p\right) + \chi_{RR}^\pm\left(\nu,a_0^{-1}p\right) + \chi_{LR}^\pm\left[\nu,a_0^{-1}(p-2k_F)\right] + \chi_{RL}^\pm\left[\nu,a_0^{-1}(p+2k_F)\right], \tag{E5}$$

with

$$\chi_{ll'}^\pm(\nu q) = -\pi\int\frac{d\omega}{2\pi}\int\frac{dk}{2\pi}[\rho_l^\pm(\omega k)\rho_{l'}^+(\omega-\nu;k-q) - \rho_l^\mp(\omega k)\rho_{l'}^-(\omega-\nu;k-q)], \tag{E6}$$

and substituting the expressions for $\rho_l^\pm(\omega k)$, we obtain Eqs. (28).

[1] P. Ribeiro, Q. Si, and S. Kirchner, Europhys. Lett. **102**, 50001 (2013).
[2] P. Ribeiro, F. Zamani, and S. Kirchner, Phys. Rev. Lett. **115**, 220602 (2015).
[3] A. Levchenko, T. Micklitz, Z. Ristivojevic, and K. A. Matveev, Phys. Rev. B **84**, 115447 (2011).
[4] T. Micklitz and A. Levchenko, Phys. Rev. Lett. **106**, 196402 (2011).
[5] T. Micklitz, A. Levchenko, and A. Rosch, Phys. Rev. Lett. **109**, 036405 (2012).
[6] S. Datta, *Electronic Transport in Mesoscopic Systems* (Cambridge University Press, Cambridge, 1995).
[7] J. Imry, *Introduction to Mesoscopic Physics*, Mesoscopic Physics and Nanotechnology (Oxford University Press, Oxford, 1997).
[8] M. Di Ventra, *Electrical Transport in Nanoscale Systems* (Cambridge University Press, Cambridge, 2008).
[9] A. Kamenev, *Field Theory of Non-Equilibrium Systems* (Cambridge University Press, Cambridge, 2011).
[10] R. Landauer, IBM J. Res. Dev. **1**, 223 (1957).
[11] M. Büttiker, Phys. Rev. Lett. **57**, 1761 (1986).
[12] D. B. Gutman, Y. Gefen, and A. D. Mirlin, Phys. Rev. Lett. **101**, 126802 (2008).
[13] D. B. Gutman, Y. Gefen, and A. D. Mirlin, Phys. Rev. B **80**, 045106 (2009).
[14] S. N. Dinh, D. A. Bagrets, and A. D. Mirlin, Phys. Rev. B **81**, 081306 (2010).
[15] S. Takei, M. Milletarì, and B. Rosenow, Phys. Rev. B **82**, 041306 (2010).
[16] D. B. Gutman, Y. Gefen, and A. D. Mirlin, J. Phys. A: Math. Theor. **44**, 165003 (2011).
[17] V. Popkov, M. Salerno, and G. M. Schütz, Phys. Rev. E **85**, 031137 (2012).
[18] A. M. Lunde, K. Flensberg, and L. I. Glazman, Phys. Rev. B **75**, 245418 (2007).

[19] J. Rech, T. Micklitz, and K. A. Matveev, Phys. Rev. Lett. **102**, 116402 (2009).
[20] A. M. Lunde, A. D. Martino, A. Schulz, R. Egger, and K. Flensberg, New J. Phys. **11**, 023031 (2009).
[21] H. Pothier, S. Guéron, N. O. Birge, D. Esteve, and M. H. Devoret, Phys. Rev. Lett. **79**, 3490 (1997).
[22] H. Pothier, S. Guéron, N. O. Birge, D. Esteve, and M. H. Devoret, Z. Phys. B: Condens. Matter **103**, 313 (1997).
[23] A. Anthore, F. Pierre, H. Pothier, and D. Esteve, Phys. Rev. Lett. **90**, 076806 (2003).
[24] Y.-F. Chen, T. Dirks, G. Al-Zoubi, N. O. Birge, and N. Mason, Phys. Rev. Lett. **102**, 036804 (2009).
[25] J.-P. Brantut, J. Meineke, D. Stadler, S. Krinner, and T. Esslinger, Science **337**, 1069 (2012).
[26] J. Lancaster and A. Mitra, Phys. Rev. E **81**, 061134 (2010).
[27] J. Lancaster, T. Giamarchi, and A. Mitra, Phys. Rev. B **84**, 075143 (2011).
[28] T. Sabetta and G. Misguich, Phys. Rev. B **88**, 245114 (2013).
[29] D. Bernard and B. Doyon, J. Phys. A: Math. Theor. **45**, 362001 (2012).
[30] D. Bernard and B. Doyon, Ann. Henri Poincare **16**, 113 (2014).
[31] P. Calabrese, C. Hagendorf, and P. L. Doussal, J. Stat. Mech. (2008) P07013.
[32] V. Eisler and Z. Rácz, Phys. Rev. Lett. **110**, 060602 (2013).
[33] V. Alba and F. Heidrich-Meisner, Phys. Rev. B **90**, 075144 (2014).
[34] Y. Ogata, Phys. Rev. E **66**, 016135 (2002).
[35] D. Karevski and T. Platini, Phys. Rev. Lett. **102**, 207207 (2009).
[36] L. Vidmar, D. Iyer, and M. Rigol, Phys. Rev. X **7**, 021012 (2017).
[37] V. Eisler and Z. Zimborás, Phys. Rev. A **89**, 032321 (2014).
[38] J. Viti, J.-M. Stéphan, J. Dubail, and M. Haque, Europhys. Lett. **115**, 40011 (2016).
[39] A. D. Luca, G. Martelloni, and J. Viti, Phys. Rev. A **91**, 021603 (2015).
[40] I. Gierz, J. C. Petersen, M. Mitrano, C. Cacho, I. C. E. Turcu, E. Springate, A. Stöhr, A. Köhler, U. Starke, and A. Cavalleri, Nat. Mater. **12**, 1119 (2013).
[41] F. Cilento, S. D. Conte, G. Coslovich, S. Peli, N. Nembrini, S. Mor, F. Banfi, G. Ferrini, H. Eisaki, M. K. Chan, C. J. Dorow, M. J. Veit, M. Greven, D. van der Marel, R. Comin, A. Damascelli, L. Rettig, U. Bovensiepen, M. Capone, C. Giannetti, and F. Parmigiani, Nat. Commun. **5**, 4353 (2014).
[42] T. Giamarchi, *Quantum Physics in One Dimension*, International Series of Monographs on Physics (Clarendon, Oxford, 2004).
[43] P. Ribeiro and V. R. Vieira, Phys. Rev. B **92**, 100302 (2015).
[44] I. Klich and L. Levitov, Phys. Rev. Lett. **102**, 100502 (2009).
[45] H. F. Song, S. Rachel, and K. Le Hur, Phys. Rev. B **82**, 012405 (2010).
[46] H. F. Song, C. Flindt, S. Rachel, I. Klich, and K. Le Hur, Phys. Rev. B **83**, 161408 (2011).
[47] H. F. Song, S. Rachel, C. Flindt, I. Klich, N. Laflorencie, and K. Le Hur, Phys. Rev. B **85**, 035409 (2012).
[48] L. S. Levitov and G. B. Lesovik, JETP Lett. **58**, 230 (1993).
[49] A. R. Its and V. E. Korepin, J. Stat. Phys. **137**, 1014 (2009).
[50] F. Ares, J. G. Esteve, F. Falceto, and E. Sánchez-Burillo, J. Phys. A: Math. Theor. **47**, 245301 (2014).
[51] R. Claessen, M. Sing, U. Schwingenschlögl, P. Blaha, M. Dressel, and C. S. Jacobsen, Phys. Rev. Lett. **88**, 096402 (2002).
[52] M. Sing, U. Schwingenschlögl, R. Claessen, P. Blaha, J. M. P. Carmelo, L. M. Martelo, P. D. Sacramento, M. Dressel, and C. S. Jacobsen, Phys. Rev. B **68**, 125111 (2003).
[53] J. M. P. Carmelo, D. Bozi, and K. Penc, J. Phys.: Condens. Matter **20**, 415103 (2008).
[54] B. Thielemann, C. Rüegg, H. M. Rønnow, A. M. Läuchli, J.-S. Caux, B. Normand, D. Biner, K. W. Krämer, H.-U. Güdel, J. Stahn, K. Habicht, K. Kiefer, M. Boehm, D. F. McMorrow, and J. Mesot, Phys. Rev. Lett. **102**, 107204 (2009).
[55] P. Bouillot, C. Kollath, A. M. Läuchli, M. Zvonarev, B. Thielemann, C. Rüegg, E. Orignac, R. Citro, M. Klanjšek, C. Berthier, M. Horvatić, and T. Giamarchi, Phys. Rev. B **83**, 054407 (2011).
[56] M. Braden, Y. Sidis, P. Bourges, P. Pfeuty, J. Kulda, Z. Mao, and Y. Maeno, Phys. Rev. B **66**, 064522 (2002).
[57] R. Werner and V. J. Emery, Phys. Rev. B **67**, 014504 (2003).
[58] K. Iida, M. Kofu, N. Katayama, J. Lee, R. Kajimoto, Y. Inamura, M. Nakamura, M. Arai, Y. Yoshida, M. Fujita, K. Yamada, and S.-H. Lee, Phys. Rev. B **84**, 060402 (2011).
[59] G. Veeravalli, E. Kuhnle, P. Dyke, and C. J. Vale, Phys. Rev. Lett. **101**, 250403 (2008).
[60] N. Fabbri, D. Clément, L. Fallani, C. Fort, and M. Inguscio, Phys. Rev. A **83**, 031604 (2011).
[61] N. Fabbri, S. D. Huber, D. Clément, L. Fallani, C. Fort, M. Inguscio, and E. Altman, Phys. Rev. Lett. **109**, 055301 (2012).
[62] R. Ozeri, N. Katz, J. Steinhauer, and N. Davidson, Rev. Mod. Phys. **77**, 187 (2005).
[63] D. Husmann, S. Uchino, S. Krinner, M. Lebrat, T. Giamarchi, T. Esslinger, and J.-P. Brantut, Science **350**, 1498 (2015).
[64] F. D. M. Haldane, Phys. Rev. Lett. **45**, 1358 (1980).
[65] F. D. M. Haldane, J. Phys. C: Solid State Phys. **14**, 2585 (1981).
[66] J. Voit, Rep. Prog. Phys. **58**, 977 (1995).
[67] M. Fabrizio and A. O. Gogolin, Phys. Rev. B **51**, 17827 (1995).
[68] A. Imambekov and L. I. Glazman, Phys. Rev. Lett. **100**, 206805 (2008).
[69] A. Imambekov, T. L. Schmidt, and L. I. Glazman, Rev. Mod. Phys. **84**, 1253 (2012).